Available online at www.dergipark.org.tr/en

INTERNATIONAL ADVANCED RESEARCHES
and
ENGINEERING JOURNAL

Journal homepage: www.dergipark.org.tr/en/pub/iarej

e-ISSN: 2618-575X

International Open Access

Volume 04
Issue 02

August, 2020

Research Article

Numerical analysis of the harvester having toroidal structure and examination of the application results

Mahmut Kabakulak [a,*] ***and Serdal Arslan*** [a]

[a]*Department of Electricity, Vocational School, Harran University, Turkey*

ARTICLE INFO

Article history:
Received 26 February 2020
Revised 22 April 2020
Accepted 26 April 2020

Keywords:
Ansys Maxwell
Energy harvesting
Electromagnetic field
Toroidal core

ABSTRACT

In most places with energy transmission, data of the line can be obtained with sensors. However, in recent years, the energy requirement of sensors has been met through harvesters. The electrical power required for sensor systems can be provided through electromagnetic fields around the line, especially through the electrical power transmission line or energy-carrying cable systems. In this study, numerical analysis of the harvester with toroidal coil, which was intended to be used for sensor feeds, was performed using Ansys Maxwell. In addition, experimental studies of the harvesters with toroidal core were carried out. The results were compared with some studies in the literature. Considering line current and saturation effects, it was seen that the studied toroid models were appropriate for home sensor applications.

1. Introduction

Today, in addition to fossil fuel energy systems, alternative energy sources have become widespread due to both increasing energy demand and environmental pollution [1, 2]. This has increased the number of power transmission and distribution lines. Due to the widespread use of overhead power lines in energy transmission and distribution, it is important to follow the lines and reduce the failures in order to increase the energy continuity and reliability on the lines as the system infrastructure ages. In order to maintain the safe transmission of energy, power lines need to be checked regularly. This is usually done directly (visual inspection), indirectly (wireless status monitoring systems) and by helicopter video inspection. In terms of other applications, a free transmission line control system, where an unmanned air vehicle conducts all activities and when doing this, it is charged from the line through the energy harvester, has been proposed [3]. For example, in China, the weight of a vibration device and the weight of a universal device is limited to 1 kg and 2.5 kg, respectively [4]. The problem can be solved by increasing the power density of the energy harvester. Wired monitoring systems are not widely used today since they require expensive communication especially over long distances [5]. Existing systems are based on the weather-data collection method used to estimate icing conditions. On the other hand, optical measurement allows the detection of the icing process by the direct measurement system depending on energy harvesting based on other methods such as microwaves and ultrasound measurement [5]. In a study, various methods such as lightning current measurement systems using current detectors, cathode-ray oscillography, cathode-ray oscillography, and Rogowski coils were examined and a new lightning current measurement system based on energy harvesters was proposed [6]. Partial discharge sensors can be utilized to monitor partial discharges of transformers using the harvester [7]. Reducing air pollution hazards and keeping particulate matter data at specific limits are of vital importance. For air-based data, a cheap wirelessly connected sensor system, which is positioned individually on the conductors of overhead power lines, has been proposed [8]. White et al. [8] conducted tests by using a printed circuit board containing ozone, carbon monoxide, temperature and humidity sensors, as well as a Bluetooth, power management circuit, and a harvesting coil. In order to obtain a higher power density in electromagnetic

* Corresponding author. Tel.: +90 414 318 30 00.
E-mail addresses: m.kabakulak@harran.edu.tr *(M. Kabakulak)*, serdalarslan@harran.edu.tr *(S. Arslan)*
ORCID: 0000-0002-0016-6735 *(M. Kabakulak)*, 0000-0002-1187-5633 *(S. Arslan)*
DOI: 10.35860/iarej.694834

harvesting applications, a material with high saturation flux density is preferred [4]. Test results for various core applications are given in Table 1. If the toroidal core volume and outer diameter are constant, the smaller the inner diameter, the greater the maximum output power [9]. The output power increases as the difference between the outer diameter and the inner diameter of the toroidal coil used for harvesting increases. In addition, the output power increases as the toroidal height increases [9]. The diameter change affects the power change more than the change in height. The presence and increase of the air gap in the toroid decrease the output power. In order to obtain maximum output power in toroidal core applications, inner resistance of the coil should not be larger than the load resistance [9]. In addition, the number of smaller turns is preferable when the line current is large [9]. The structure of the energy harvesting device shown in Figure 1 consists of toroidal core with winding placed on the harvesting line. Power line generates a magnetic field around the core. The magnetic field density, generated in the coil, produces indirect proportion to the magnetic permeability of the core and the harvester produces a voltage induced in the coil [10]. In fact, based on the basic principle of the induction voltage with variable magnetic field over time, the induced voltage is directly proportional to the magnetic permeability of the core material [10]. The higher the core permeability, the larger the magnetic permeability of the core; it is important to note that the induced electric voltage is so high. By using a material with high magnetic permeability, a smaller magnetic core can provide high power density. Due to the high permeability of the ferrite and iron powder alloy, the nanocrystalline core is recommended for compact, autonomous magnetic induction-based energy harvesting devices because of its high power density [10]. However, when current is high, the flux density in the core no longer changes or it changes very slowly due to the vacuum permeability. When it is saturated, the inductance of the inductor approaches zero and very little energy is harvested [11]. Therefore, to be able to study the behavior of the core, an accurate model should be established [11].

Table 1. Test results for various core applications

Ref.	Core Material	Line Current (A)	Harvested Power (mW)	Shape
[4]	Si-steel	10	350	Toroid
[10]	Ferrite	5	16.8	Toroid
[10]	Nano-crystalline	5	9	Toroid
[10]	Iron powder	5	-	Toroid
[8]	Si-steel	100	0.0015	U Core
[9]	Si-steel	102.5	0.01764	Toroid

In the literature, multiple circuits have been proposed for wireless charging systems. Usually, the AC/DC rectifier has been proposed for energy harvesting from power-module transmission lines, including power matching, digital logical unit, and supercapacitors used to store harvested energy [12]. Batteries are used as the primary sources to ensure the full functionality of the high-voltage wireless sensor node in power lines. In addition, batteries are used to support the functionality of the test and debugging unit during the field-testing phase [12]. However, while increasing the life and safety of the sensor system, harvesters can also serve as a unique source without a battery [13].

As a continuation of our previous studies [14-17], the electromagnetic harvester with a toroidal structure was examined in this study. Harvesters with different toroidal structures were compared with similar studies in the literature. Section two provides information about the features of the model and methodology of the study. In section three, numerical analysis of toroidal type models and the data of the experiment are examined and the results are discussed in the final section.

2. Materials and Method

In Figure 1, drawings of the toroidal model are given. Here, "D_0" refers to outer diameter, "D_i" refers to inner diameter and "L" refers to thickness. The harvesters with toroidal amorphous materials, whose technical specifications are given in Table 2, were studied. For these models whose numerical analysis was done with the Ansys Maxwell software, experiments were conducted by installing the experiment set shown in Figure 2. Then, the experimental data and numerical analyses were compared.

The mean magnetic flux pathway (L_{mT}) for Toroidal nudes is calculated using Equation 1 [18]:

$$L_{mT} = \frac{\pi(D_0 - D_i)}{\ln\left(\frac{D_0}{D_i}\right)} \quad (1)$$

If the winding length for the toroidal cores is written as L_{TB}, Equation 2 is obtained.

$$L_{TB} = (D_0 - D_i) + 4r + 2L \quad (2)$$

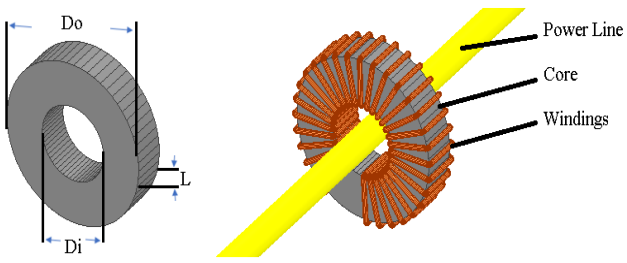

Figure 1. General structure of the toroidal-core model harvester

Table 2. Technical characteristics of the toroidal type harvester models

Models	Do (mm)	Di (mm)	L (mm)	N (number of turns)	Wire Diameter (mm)	Calculation Rdc (Ω)	Measured (LCR meter) Rdc (Ω)	Measured (LCR meter) L (H)
Model 1	55	37	30	91	0.95	0.19	0.23	0.745
Model 2	52	32	20	91	0.50	0.51	0.60	0.505
Model 3	42	24	16	91	0.50	0.43	0.49	1.232

where r is the conductor diameter, ρ is resistivity, S is cross-sectional area of the copper wire, N is the number of turns in the coil and L is the core thickness. Equation 3, which is the calculation of winding resistance, is obtained approximately for these toroidal cores.

$$R = \rho \frac{(D_0 - D_i) + 4r + 2L}{S} N \quad (3)$$

Core losses at various frequency and induction levels are measured using various excitation waveforms. Based on measurements [18], the coefficients of the Steinmetz Equation (4) are estimated:

$$P_w = k_w (f / f_0)^{\alpha} (B / B_0)^{\beta} \quad (4)$$

where P_w is the core loss per unit weight, f_0 is the basic frequency (1 Hz), and B_0 is the basic flux density (1 T). Also, k_w, α, and β are Steinmetz coefficients derived from experimental data. When the waveform was sinusoidal, the coefficients were taken as kw=0.003369, α=1.301033, and β=2.135959 [18]. The images of the toroidal model harvesters in the experiment set are given in Figure 2.

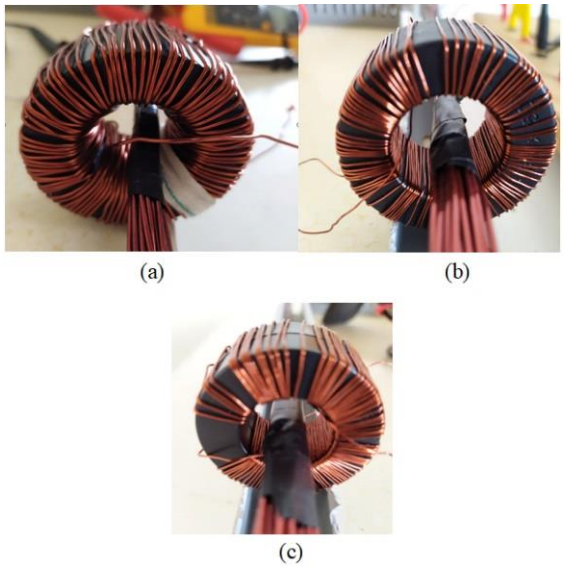

Figure 2. Images of toroidal models in the experiment set; (a) Model 1, (b) Model 2, (c) Model 3

The experimental setup created for the energy harvesting system is given in Figure 3. The materials in this experiment set are listed as load group, power line, and harvester cores. In order to pass current through the line, the load group consisting of incandescent lamps was connected in different ways (series and parallel) between itself, and the line current was generated; then, this current was measured with a clamp multimeter and recorded. To increase the line current and magnetic field density around the line, the number of conductors on the line was increased.

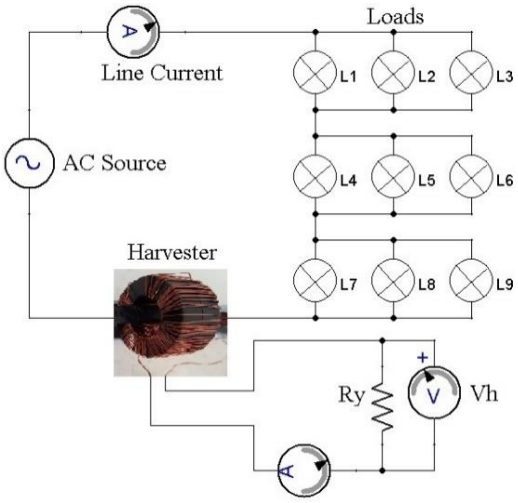

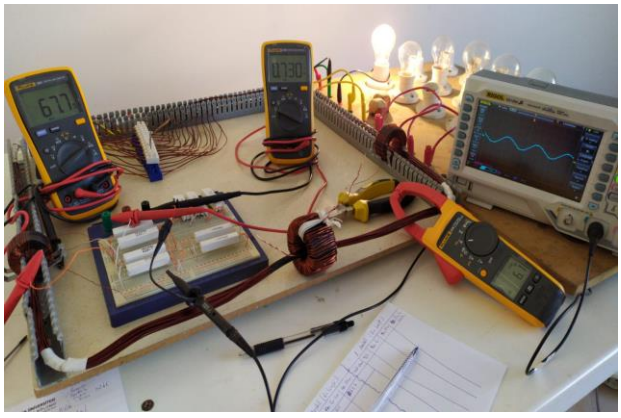

Figure 3. (a) Electrical circuit diagram of the experimental setup, (b) Harvester experimental setup

The line conductor was wrapped with more than one winding on a rectangular wooden floor by using cable channel. The cores in the toroidal geometry used for energy harvesting (Figure 2) were placed on the line. In this experiment set (Figure 3), the voltages and currents harvested at different loads from the harvesters were measured with multimeters and recorded.

Experiments of toroidal type models having amorphous structure were carried out in the experimental setup (Figure 3) where the electrical line was modeled. 3 A, 6.2 A and 9.2 A were passed on the line respectively, the harvester load (Ry) was also changed between 11 Ω and 330 Ω, and the current and voltage harvested at different line currents and at different loads were measured and recorded. The harvested power is calculated by multiplying the harvested current and voltage. Harvested current, voltage and power graphs of the data recorded in the excel file were obtained according to the load.

3. Numerical Analysis of the Toroidal Models and Data of the Experiment

Solving complex structures with finite element method (FEM) provides both high accuracy and time savings. Therefore, in the study, ANSYS Maxwell commercial software, which is using FEM, is used because it has wide drawing and solver (Transient, Magnetostatic, Eddy current, etc.) infrastructure. This program creates subregions in the structure by dividing the structure into multiple tetrahedron pieces to determine the magnetic field in nonhomogeneous structures. It determines the area of each region with separate polynomials for each subregion. In case the core material is not linear, analysis is done by using the B-H curve with a linear approach by Newton-Raphson method. After the analysis is completed, error analysis is carried out, and the solver continues to analyze the faulty finite element repeatedly until the determined criteria are fulfilled. As a result, magnetic field intensity, magnetic flux density, inductance values and forces can be obtained for materials determined with this software [19, 20]. The software uses the Ampere's law and Maxwell's equations in the static field solution of electromagnetic problems [22, 23]. Gauss' law is considered in magnetostatic analysis. Equation 5 between magnetic field intensity (*B*) and magnetic field intensity (*H*) is given in:

$$H = \frac{B}{\mu_o \, \mu_r} \tag{5}$$

Here μ_o and μ_r are the permeability of the vacuum and relative permeability of material, respectively. The curl of the vector potential (*A*), is defined as Equation 6, gives us the magnetic field:

$$\vec{B} = \nabla \times \vec{A} \tag{6}$$

J is the conduction current density. Equation 7 is defined as the Ampere's law.

$$\nabla \times \vec{H} = \vec{J} \tag{7}$$

Equation 8 is derived using Equation 5 and Equation 6. Thus, the software solves Equation 8 using the finite element method.

$$\nabla \times \left(\frac{1}{\mu_o \, \mu_r} \nabla \times \vec{A}\right) = \vec{J} \tag{8}$$

Line current (6.2 A) of the Model 1, whose technical specifications are given in Table 2, was determined and static magnetic analysis of it was performed with Ansys Maxwell. In Figure 4, the magnetic flux density change of the core and results of the flux lines analysis are shown.

Determinations were made such that 6.2 A-line current would pass through the middle of the Toroidal model. The magnetic flux density value for this model is the value of 1.35 T at most. This flux density decreases towards the outside of the toroidal. In addition, because the toroidal model consists of a single piece, magnetic flux lines do not deteriorate and leakage fluxes do not occur. The iron loss was calculated using the Steinmetz formula given in Equation 4. This loss was 0.89 Watts on average.

The graph of the harvested-power (Ph) change by the change of line current (I_{line}) and load resistance (R_y) in the experiments conducted for Model 1 is given in Figure 5. The maximum harvested power at 3 A line current was measured as 96.77 mW at 235 Ω load-resistance. The maximum power at 6.2 A line current was measured as 277.98 mW at 88 Ω load-resistance. The maximum power at 9.2 A line current was measured as 443.78 mW at 55 Ω load-resistance. As seen in the experimental data, as the line current increases, the load-resistance at which the maximum harvested power occurs decreases.

The graph of the harvested-voltage (Vh) change by the change of line current (I_{line}) and load resistance (Ry) in the experiments conducted for Model 1 is given in Figure 6. In cases where line current was 3 A and 6.2 A, as the harvester load increased, the harvested voltage increased too. At 9.2 A line current, the harvested voltage increased up to 235 Ω load-resistance, then as the load increased, the harvested voltage began to drop.

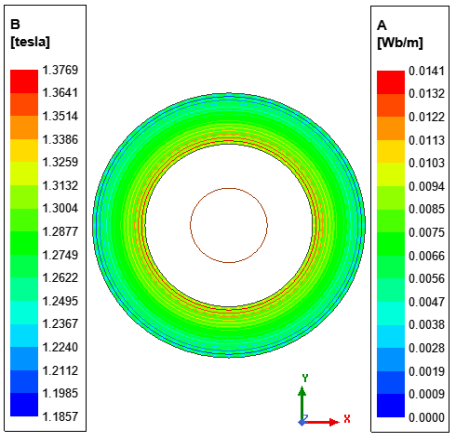

Figure 4. Model 1; magnetic flux density change and flux lines

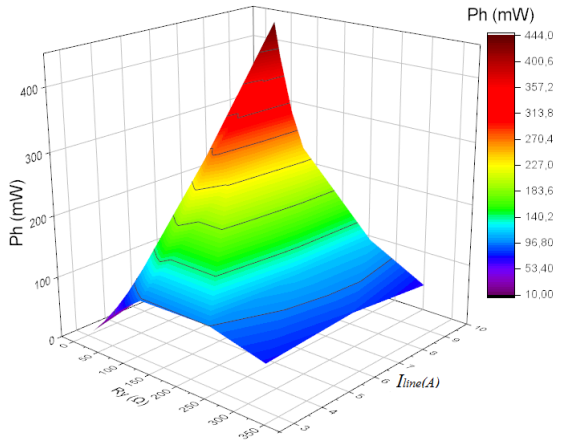

Figure 5. Harvested power change graph for Model 1

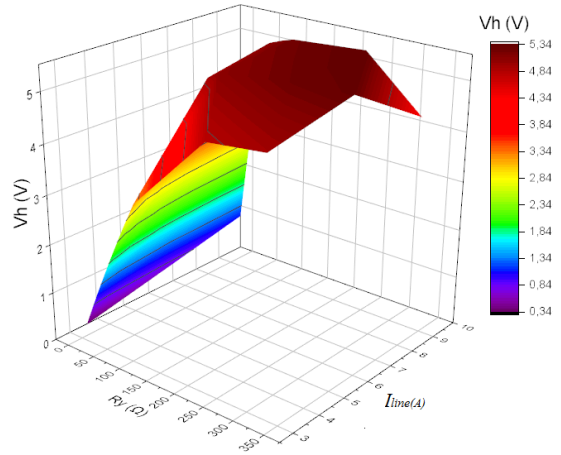

Figure 6. Harvested voltage change graph for Model 1

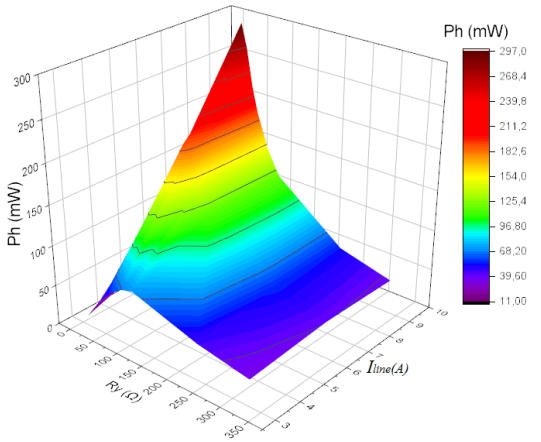

Figure 7. The harvested power change graph for Model 2

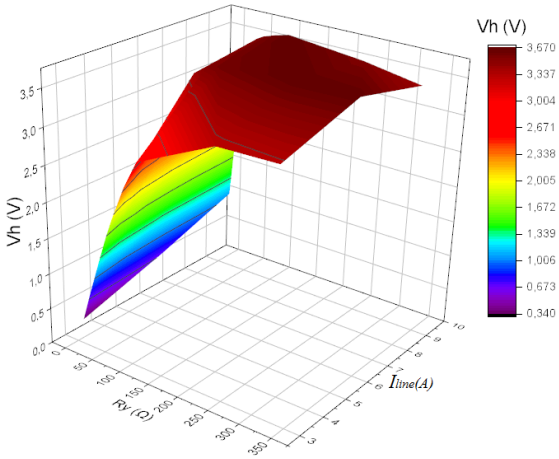

Figure 8. The harvested voltage change graph for Model 2

The graph of the harvested-power (Ph) change by the change of line current (I_{line}) and load resistance (Ry) in the experiments conducted for Model 2 is given in Figure 7. The maximum harvested power at 3 A line current was measured as 71.69 mW at 110 Ω load-resistance. The maximum power at 6.2 A line current was measured as 188.80 mW at 55 Ω load-resistance. The maximum power at 9.2 A line current was measured as 296.36 mW at 33 Ω load-resistance. As seen in the experimental data, as the line current increases, the load-resistance at which the maximum harvested power occurs decreases.

The graph of the harvested-voltage (Vh) change by the change of line current (I_{line}) and load resistance (Ry) in the experiments conducted for Model 2 is given in Figure 8. In cases where line current was 3 A and 6.2 A, as the harvester load increased, the harvested voltage increased too. At 9.2 A line current, the harvested voltage increased up to 150 Ω load-resistance, then as the load increased, the harvested voltage began to drop.

The graph of the harvested-power (Ph) change by the change of line current (I_{line}) and load resistance (Ry) in the experiments conducted for Model 3 is given in Figure 9. The maximum harvested power at 3 A line current was measured as 52.56 mW at 55 Ω load-resistance.

The maximum power at 6.2 A line current was measured as 99.26 mW at 22 Ω load-resistance. The maximum power at 9.2 A line current was measured as 132.04 mW at 15 Ω load-resistance. As seen in the experimental data, as the line current increases, the load-resistance at which the maximum harvested power occurs decreases.

The graph of the harvested-voltage (Vh) change by the change of line current (I_{line}) and load resistance (Ry) in the experiments conducted for Model 3 is given in Figure 10. In cases where line current was 3 A, as the harvester load increased, the harvested voltage increased too. At 6.2 A line current, the harvested voltage increased up to 235 Ω load resistance and then load values began to decrease. At 9.2 A line current, the harvested voltage increased up to 110 Ω load-resistance, then as the load increased, the harvested voltage began to decrease.

As seen in the experimental data, as the line current increases, the load-resistance at which the maximum harvested power occurs decreases. The reason for this condition can be based on equal in load impedance value to the equivalent source resistance. In the total impedance calculation of the harvester, since the magnitude of the coil-winding resistance is very small compared to the resistance generated by the core losses, those creating the actual impedance are core losses. Therefore, as the line current

increases, the load at which the maximum power occurs in the harvester decreases [4].

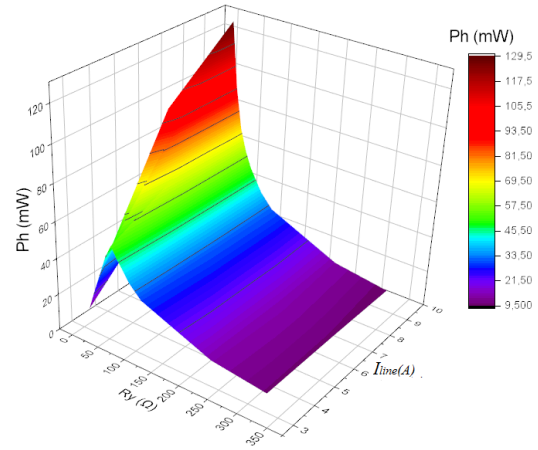

Figure 9. The harvested power change graph for Model 3

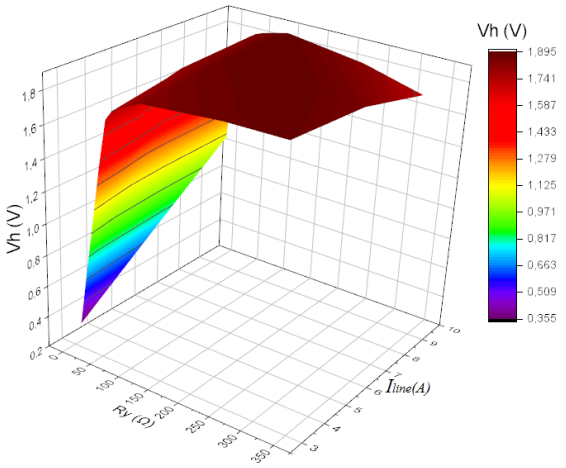

Figure 10. The harvested voltage change graph for Model 3

The harvested power change graph, which was combined according to load change in experiments conducted on 9.2 A line current of toroidal models, is given in Figure 11. When the graphs of the toroidal type models were examined, it was observed that as the harvester load increased, the harvested current decreased, and the harvested voltage increased up to a certain load value. However, the harvested power reached its maximum at a certain load value. Since there is no air gap in the structures of the toroidal cores, more magnetic flux passes over them.

As seen in the graphs, as the line current increased, more power was harvested, but the core reached saturation at smaller loads. The power and output voltage changes with the reduced permeability in the saturated magnetic core [21].

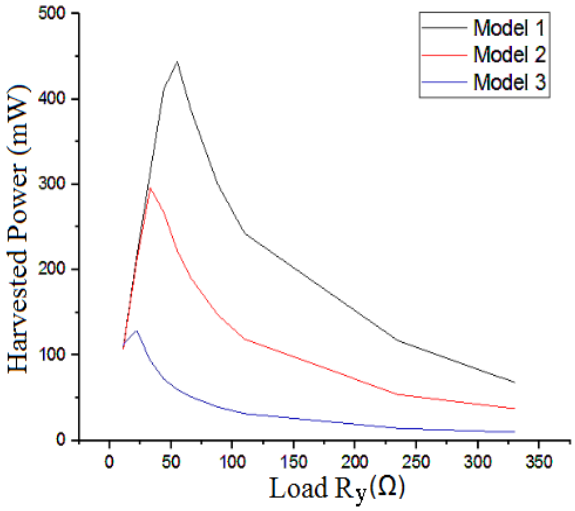

Figure 11. The harvested power change graph in toroidal models

Table 3. Comparison of power densities

Study	Core Material	Line Current (A)	Ry (Ω)	Number of Winding	D_0	D_i	$\frac{Do - Di}{2}$	L	Power Density (mW/cm^3)
[10]	Ferrite	5	-	156	36	23	6.5	15	7.83
[10]	Nanocrystalline	5	-	96	33.5	27.5	3	4	1.98
[10]	Iron powder	5	-	111	38.4	21.5	8.45	11.1	0
[4]	Silicon steel	5	900	200	75	55	10	30	2.38
This study Model 1	Amorphous	6.2	88	92	54	37	8.5	30	7.63
This study Model 2	Amorphous	6.2	55	92	50	32	9	20	8.14
This study Model 3	Amorphous	6.2	22	92	40	25	7.5	15	8.64
[4]	Silicon steel	10	770	200	75	55	10	30	9.54
This study Model 1	Amorphous	9.2	55	92	54	37	8.5	30	12.18

In a way supporting previous studies [4, 10], it was seen that Model 1 harvested more power due to the greatness of its volume and its smaller internal diameter than the Model 2. The fact that the volume of Model 3 was very small caused it to reach saturation at smaller loads and led less power to be harvested. In Table 3, the comparison of the power density of the models examined in this study with the previous studies on toroidal geometric harvesters is given.

When Table 3 was examined, it was seen that compared to the ferrite-core harvester, 10.34% more power density was obtained from the amorphous-core model 3 harvester with approximately the same line current and approximately the same internal diameters. Again, when the power densities of the Model 3 harvester and the nanocrystalline harvester with approximately the same line current and approximately the same internal diameters were compared, it was observed that approximately 4.3 times more power density was obtained from the Model 3 harvester with the amorphous core. When the power density of the harvester, which had 10 A line current and silicon steel material, was compared with the Model 1 9.2 A line-current harvester with amorphous material, it was figured out that 27.67% more power density was obtained from the Model 1 harvester. Again, when Table 3 is examined, it is understood that although the power density is independent of the number of winding, the magnitude of the line current affects it. Considering the same line current and winding number, although the power value of the Model 1 is the highest in Figure 11, it is the smallest in terms of power density.

4. Conclusions

When the toroidal models in this study were compared, it was seen that from the harvesters with the same core material and the same line current, more power density was obtained in the Model with a lower internal diameter. In this context, more power density was obtained from the Model 3 harvester, where the internal diameter, hence the air gap between the line and the harvester, was the lowest. When the same line current and winding numbers are taken into account, the values, at which the output power of the discussed models are maximum, change. Especially for core designs with a toroidal structure or closed flux path, the operating current can create saturation in the core material. Therefore, it is essential to perform the numerical analysis of the system to be studied by taking the line current into account. In addition, in the literature, due to its very low magnetic permeability, the iron-powder core material is not considered appropriate for use in harvesters. However, the harvester with amorphous material has been found to be appropriate for sensor systems. However, the system should be designed taking into account the saturation effects. In terms of future studies, experiments will be carried out on the operation of the toroid-structured model in the home sensor application. In addition, studies on special and different types of harvester models will also be performed.

Declaration

The author(s) declared no potential conflicts of interest with respect to the research, authorship, and/or publication of this article. The author(s) also declared that this article is original, was prepared in accordance with international publication and research ethics, and ethical committee permission or any special permission is not required.

Acknowledgment

This study was produced from the master's thesis prepared by the first author under the supervision of the second author.

This work supported by the Scientific Research Project Unit of the Harran University under Research Project (project no: 18060), Turkey.

References

1. Yilmaz, C., and M. Kanoglu, *Investigation of hydrogen production cost by geothermal energy*. International Advanced Researches and Engineering Journal, 2017. **1**(1): p. 5-10.
2. Sen, O., and C. Yilmaz, *Thermodynamic performance analysis of geothermal and solar energy assisted power generation and residential cooling system*. International Advanced Researches and Engineering Journal, 2020. **4**(1): p. 41-47.
3. Boles, J.D., et al. *Inductive power harvesting for a touchless transmission line inspection system*. in *IEEE Power and Energy Society General Meeting (PESGM) 2016:* Boston, USA. p.1-5.
4. Liu, Y., et al., *A novel high-density power energy harvesting methodology for transmission line online monitoring devices.* Review of Scientific Instruments, 2016. **87**(7): p. 075119.
5. Moser, M.J., et al., *Strong and weak electric field interfering: Capacitive icing detection and capacitive energy harvesting on a 220-kV high-voltage overhead power line.* IEEE transactions on industrial electronics, 2010. **58**(7): p. 2597-2604.
6. Yang, F., et al., *A novel self-powered lightning current measurement system.* IEEE Transactions on Industrial Electronics, 2017. **65**(3): p. 2745-2754.
7. Yuan, S., et al., *A high-efficiency helical core for magnetic field energy harvesting.* IEEE Transactions on Power Electronics, 2016. **32**(7): p. 5365-5376.
8. White, R.M., et al., *Atmospheric sensors and energy harvesters on overhead power lines.* Sensors, 2018. **18**(1): p. 114.
9. Wang, W., et al., *Optimization design of an inductive energy harvesting device for wireless power supply system overhead high-voltage power lines.* Energies, 2016. **9**(4): p. 242.
10. Dos Santos, M.P., et al. *Energy harvesting using magnetic induction considering different core materials*. in *2014 IEEE International Instrumentation and Measurement Technology Conference (I2MTC)*2014:Montevideo, Uruguay. p.1-3.

11. Zhuang, Y., et al. *An improved energy harvesting system on power transmission lines*. in *IEEE Wireless Power Transfer Conference (WPTC)*2017: Taipei, Taiwan. p.1-3.
12. Zhao, X., et al. *Energy harvesting for overhead power line monitoring*. in *International Multi-Conference on Systems, Signals & Devices* 2012: Chemnitz, Germany. p.1-5.
13. Çelik, K., E. Kurt, and Y. Uzun, *Experimental and theoretical explorations on the buckling piezoelectric layer under magnetic excitation.* Journal of Electronic Materials, 2017. **46**(7): p. 4003-4016.
14. Kabakulak, M., M.T. Güllüoğlu, and S. Arslan. *A wireless energy harvesting system design and numerical analysis.* in *3rd International Congress of Professional and Technical Sciences* 2018: Gaziantep, Turkey. p.418-425.
15. Kabakulak, M., M.T. Güllüoğlu, and S. Arslan. *Energy harvester analysis in common simulation platform*. in *1st International GAP Mathematics - Engineering - Science and Health Sciences Congress*2018: Sanliurfa, Turkey. p. 26-32.
16. Kabakulak, M., M.T. Güllüoğlu, and S. Arslan. *Comparison of energy harvesters according to change of conductor form*. in *1st International Mersin Symposium* 2018: Mersin, Turkey. p.16-26.
17. Kabakulak, M., M.T. Güllüoğlu, and S. Arslan. *Energy Harvesting from Busbar*. in *1st International Mersin Symposium*2018: Mersin, Turkey. p.27-36
18. *METGLAS® 2605-SA1 core datasheet*. 2018 [01 January 2020]; Available from: https://www.netl.doe.gov/sites/default/files/netl-file/METGLAS-2605-SA1-Core-Datasheet_approved%5B1%5D.pdf.
19. Fenercioğlu, A., and Tarimer, I., *Solution Processes of a Magnetic System's Magnetostatic Analysis wıth Maxwell 3D Field Simulator.* Selçuk Teknik Dergisi, 2007. **6**(3): p. 221-240.
20. Arslan S., *Medium frequency spot welding transformer and machine design*. MSc Thesis, 2011, Turkey: Gazi University, Graduate School of Natural and Applied Sciences.
21. Park, B., Kim, et al. *Optimization design of toroidal core for magnetic energy harvesting near power line by considering saturation effect.* AIP Advances, 2018. **8**(5): p. 1-7.
22. Kabakulak M., *Energy harvesting from electromagnetic fields around overhead power lines*. MSc Thesis, 2020, Turkey: Harran University, Graduate School of Natural and Applied Sciences.
23. ANSYS, *Ansys Maxwell 2019 version Help File*, p.1-2955.